ISAS - INTERNATIONAL SCHOOL FOR ADVANCED STUDIES

SISSA  ISAS

SCUOLA INTERNAZIONALE SUPERIORE DI STUDI AVANZATI
INTERNATIONAL SCHOOL FOR ADVANCED STUDIES

Empirical Tight-Binding Molecular Dynamics of Silicon Systems

Thesis submitted for the degree of
"Magister Philosophiæ"

CANDIDATE
Leonardo De Maria

SUPERVISORS
Prof. Stefano Baroni
Dott. Maria Peressi
Dott. Silvia Rubini

October 1994

SISSA - SCUOLA INTERNAZIONALE SUPERIORE DI STUDI AVANZATI
TRIESTE
Strada Costiera 11

TRIESTE

A mi padre y a la memoria de mi madre.

Acknowledgements

I think everyone is completely responsible of its own decisitions; anyhow there are always people who show you the way you will finally follow. In this case Carolina Carrizosa is that person. She introduced me to Daniele Amati some years ago when he was in Bogotá on a conference and then encouraged me to come to SISSA after I got my B.Sc. .

I'm indebted to Daniele. At the very beggining of the course I was planning to give up. Without his advice I would probably have done it. I am also so very indebted to so many other people that is impossible to give here an explicit acknowledgement to all of them. Thus I apologize in advance for any omission.

First of all I would like to thank Stefano Baroni, Maria Peressi and Silvia Rubini for introducing me in the research field of this thesis. I really appreciate having been in contact with them, and I hope to have not abused of their patience. Maria's constant encouragment and availability was fundamental to complete the work.

Special thanks go to all the Students Secretariat people: Riccardo Iancer, Andrea Parma, Claudia Parma Millo, Alex Meehan Poretti and Fabia Sparagna, and to the INFM secretary Sabrina Gustin. They were always ready to help me when I was in need. As available as them were also the computer people: Roberto Innocente, Fabio Lonzar, Marina Picek and Luisa Urgias. A word of acknowledgement also goes to Franco Viviani and Fabrizio Melchionna.

SISSA condensed matter theory group represents a good environment to start with the specialization on the field. I want to thank Erio Tosatti and all the people of the sector for their help.

Last but not least are my friends, the people that I've met at Trieste in this two years: *los del lado de acá*. I thank you all, sincerely. In different ways all

of you have contributed to make a richer person of me.

I finally thank my father, Claudine and my brother, for being so close even if we were so far.

Contents

List of symbols

m	electron mass.
$-e$	electron charge.
M_k	mass of the k-th nucleus.
Z_k	charge of the k-th nucleus.
$\mathbf{r}_i$	position of the i-th electron.
$\mathbf{p}_i$	momentum of the i-th electron.
$\mathbf{R}_k$	position of the k-th nucleus.
$\mathbf{P}_k$	momentum of the k-th nucleus.
$\{\mathbf{R}\}$	set of all the nuclear positions $\{\mathbf{R}_1, ..., \mathbf{R}_N\}$.
$\{\mathbf{r}\}$	set of all the electronic positions $\{\mathbf{r}_1, ..., \mathbf{r}_M\}$.
H	hamiltonian operator of the solid.
$H_{e\ell}$	N-particle electronic hamiltonian.
$\Psi_\mu(\mathbf{r};\mathbf{R})$	N-particle electronic eigenstates.
$\Psi_0(\mathbf{r};\mathbf{R})$	N-particle electronic ground state.
$E_\mu^{e\ell}(\mathbf{R})$	eigenvalues of the N-particle electronic hamiltonian.
H_{tot}	total,$H_{e\ell}$ plus ion-ion potential energy, hamiltonian.
$E_\mu^{tot}(\mathbf{R})$	eigenvalues of the total hamiltonian
$E_0^{tot}(\mathbf{R})$	total energy of the system, eigenvalue corresponding to the ground state of H_{tot}
$\Pi_\lambda(\mathbf{R})$	N-particle ionic eigenstates.
E_λ^{ion}	N-particle ionic eigenvalues.
H_{eff}	effective one-electron hamiltonian.
$\psi_{\nu_i}(\mathbf{r}_j;\mathbf{R})$	one-electron eigenfunctions.
ε_{ν_i}	one-electron eigenvalues.
H_{eff}^{HF}	Hartree-Fock effective one-particle operator.

$T_{e\ell}$	electronic kinetic energy operator.
U_{eI}	electron-ion interaction operator.
U_H	Hartree operator.
U_X	exchange operator.
E_{KE-eI}	electronic kinetic energy plus electron-ion attractive energy.
E_{ee}	electron-electron interaction energy.
E_{II}	ion-ion interaction energy.
E_H	Hartree energy.
E_X	exchange energy.
E_{bs}	band structure energy.
E_{rep}	repulsive energy.
$V(R_{kl})$	two-body repulsive potential.
$\mathcal{U}(\mathbf{r}-\mathbf{R}_\ell)$	*spherical* atomic effectiv potential centered at atom ℓ.
$\phi_\alpha(\mathbf{r}-\mathbf{R}_\ell)$	atomic orbital centered at atom ℓ.
$C_{\nu_i\alpha l}$	expansion coefficients of the one-electron eigenfunctions $\psi_{\nu_i}(\mathbf{r}_j;\mathbf{R})$ on the set $\{\phi_\alpha(\mathbf{r}-\mathbf{R}_\ell)\}$.
ϵ_α	on-site energy integrals.
$S_{\alpha' l' \alpha l}$	overlap integrals.
$H_{\alpha' l',\alpha l}$	energy overlap elements.
$\langle \epsilon_s \rangle$	energy of the $3s$ orbital of Silicon.
$\langle \epsilon_p \rangle$	energy of the $3p$ orbital of Silicon.
$\langle ss\sigma \rangle$	hopping energy integral between $3s$ orbitals.
$\langle sp\sigma \rangle$	hopping energy integral between $3s$ and $3p$ orbitals.
$\langle pp\sigma \rangle$	hopping energy integral between $3p$ orbitals.
$\langle pp\pi \rangle$	hopping energy integral between $3p$ orbitals.
f_s	scaling function.

V^x	x structure equilibrium volume per atom.
E^x	x structure cohesive energy per atom.
B^x	x structure bulk modulus.
V_{exp}^{dia}	silicon diamond structure experimental equilibrium volume per atom.
R_c	cut-off distance of Goodwin *et al.*[9] repulsive potential.
n_c	decaying-ratio of Goodwin *et al.*[9] repulsive potential.
R_0	nearest-neighbour equilibrium distance for Silicon in the diamond structure.
V_0	value of the repulsive potential at R_0.
$\mathcal{L}$	Car-Parrinello lagrangian.
μ	fictitious mass of the electrons.
$\dot{\psi}_i(\mathbf{r})$	time derivative of the one-electron wave function $\psi_i(\mathbf{r})$.
$\dot{\mathbf{R}}_k$	time derivative of the nucleus vector position $\mathbf{R}_k$.
Λ_{ij}	Lagrange multipliers.
$\mathbf{F}_\ell$	Hellman-Feyman force acting on ion ℓ.
N_{ij}	instantaneous value of the dot product between one-electron wave function ψ_i and ψ_j.
x_e	dynamical variable controlling the thermostat acting on electrons.
$\dot{x}_e$	time derivative of x_e.
Q_e	mass of the thermostat acting on electrons.
x_R	dynamical variable controlling the thermostat acting on ions.
$\dot{x}_R$	time derivative of x_R.
Q_R	mass of the thermostat acting on ions.

$\mathcal{F}_\ell$	total force acting on ion ℓ.
$E_{kin,0}$	average fictitious kinetic energy of the electrons.
k_B	Boltzmann constant.
T	physical temperature of the simulation.
$\mathbf{h}$	matrix with the box coordinates.
$\mathbf{a}$	primitive Bravais vector.
$\mathbf{b}$	primitive Bravais vector.
$\mathbf{c}$	primitive Bravais vector.
$\mathbf{s}$	electron position vector referred to the box, $\mathbf{s} = \mathbf{h}^t\mathbf{r}$.
$\mathbf{S}$	ion position vector referred to the box, $\mathbf{S} = \mathbf{h}^t\mathbf{R}$.
G	metric tensor, $G = \mathbf{h}^t\mathbf{h}$.
Ω	instantaneous box volume, $\Omega = det(\mathbf{h})$.
W	box mass.
p	external pressure.
Π	internal strain tensor.
C_{im}	abbreviated way of writing $C_{\mu_i i\alpha}$.
Δt	time interval for numerical integration of the Car-Parrinello equations of motion.
$\mathbf{V}_\ell$	velocity of ion ℓ.

List of Figures

1 Introduction

The realization of a scheme which unifies the approaches of density functional theory and molecular dynamics [1], allowing for a quantum mechanical calculation of the interatomic forces, represents a very important advance in the field of computational condensed matter physics.

In principle fundamental and superior to any other proposed approach, in practice it requires so much computational effort that its applicability is limited to systems of approximately 100 atoms. An alternative scheme to overcome the difficulties of a fully *ab-initio* approach has been proposed. In this scheme the electronic energies and Hellman-Feynman forces are calculated by an empirical tight-binding(TB) method. The compromise between computational speed and accuracy of this so called Empirical Tight-Binding Molecular Dynamics (ETBMD) scheme is considered satisfactory.

This work is a preliminary approach to the ETBMD scheme, an exercise to learn the method and to discuss its applicability to different kinds of problems. We have choosen to study silicon, which has been widely studied both with *ab-initio* and semi-empirical methods.

The work is organized as follows: in section 2, we discuss in detail the general features of Empirical TB methods. In section 3, the problem of transferability is addressed by studying several silicon bulk structures. In section 4 we give a short general description of the Car-Parrinello scheme for molecular dynamics and then we describe briefly all the elements needed for the specific calculations we intend to do. Section 5 is devoted to the simulation of the Si(100) clean surface reconstruction. In section 6 we present the conclusions.

2 Empirical Tight-Binding methods

Each solid consists of electrons of mass m and charge $-e$, and nuclei of masses M_k and charges Z_k. The interaction between these particles is purely electromagnetic. Considering only the Coulomb interaction, i.e. neglecting other terms such as spin-orbit interaction, etc. , the hamiltonian writes

$$H = \sum_i \frac{\mathbf{p}_i^2}{2m} - \sum_{i<j} \frac{e^2}{|\mathbf{r}_i - \mathbf{r}_j|} + \sum_{i,k} \frac{Z_k e^2}{|\mathbf{r}_i - \mathbf{R}_k|} + \sum_k \frac{\mathbf{P}_k^2}{2M_k} + \sum_{k<\ell} \frac{Z_k Z_l e^2}{|\mathbf{R}_k - \mathbf{R}_\ell|}. \quad (1)$$

The lower case letters $\mathbf{r}_i$ and $\mathbf{p}_i$ are used for the coordinates and momenta of electrons, while the capital letters $\mathbf{R}_k$ and $\mathbf{P}_k$ for the corresponding quantities of the nuclei. The set of all the nuclear positions $\{\mathbf{R}_1, ..., \mathbf{R}_N\}$ will be denoted for simplicity with $\{\mathbf{R}\}$, and that of all the electronic positions $\{\mathbf{r}_1, ..., \mathbf{r}_M\}$ with $\{\mathbf{r}\}$.

In the Born-Oppenheimer approximation [2] the nuclear and electronic motions are separated allowing to handle the two eigenvalue problems independently. The electrons move in the field of the nuclei considered fixed at some positions $\{\mathbf{R}\}$. The purely electronic problem yields a complete set of electronic eigenstates $\{\Psi_\mu(\mathbf{r};\mathbf{R})\}$

$$H_{e\ell}\Psi_\mu(\mathbf{r};\mathbf{R}) = E_\mu^{e\ell}(\mathbf{R})\Psi_\mu(\mathbf{r};\mathbf{R}), \quad (2)$$

where $H_{e\ell}$ is the sum of the first three terms on the right hand side of (1). Both the eigenvalues $E_\mu^{e\ell}(\mathbf{R})$ and the eigenstates $\Psi_\mu(\mathbf{r};\mathbf{R})$ depend parametrically on the coordinates $\{\mathbf{R}\}$. It is useful to combine $H_{e\ell}$ with the ion-ion interaction term into the hamiltonian

$$H_{tot} = H_{e\ell} + \sum_{k<\ell} \frac{Z_k Z_\ell e^2}{|\mathbf{R}_k - \mathbf{R}_\ell|}, \quad (3)$$

which has the same eigenstates as $H_{e\ell}$, with energies :

$$E_\mu^{tot}(\mathbf{R}) = E_\mu^{e\ell}(\mathbf{R}) + \sum_{k<\ell} \frac{Z_k Z_\ell e^2}{|\mathbf{R}_k - \mathbf{R}_\ell|}. \quad (4)$$

The ionic problem is given by

$$\left[\sum_k \frac{\mathbf{P}_k^2}{2M_k} + E_\mu^{tot}(\mathbf{R})\right] \Pi_\lambda(\mathbf{R}) = E_\lambda^{ion} \Pi_\lambda(\mathbf{R}), \tag{5}$$

For each electronic state μ the corresponding eigenvalue $E_\mu^{e\ell}(\mathbf{R})$ plus the ion-ion interaction term act as an *effective* internuclear potential $E_\mu^{e\ell}(\mathbf{R})$.

In the first part of this work much interest will be devoted to the problem of the electronic ground state $\Psi_0(\mathbf{r};\mathbf{R})$ in correspondence to a given static configuration of ions $\{\mathbf{R}\}$. The total energy of the ground state will be given by (4) with $\mu = 0$; in the text, when used without explicit specification, *total energy* will have this meaning. The study of the quantum problem posed by (5) is not going to be carried on. In the second part of the work, devoted to dynamical simulations, the *classical* motion of the ions will be considered. The forces acting on ions will be obtained directly from the effective internuclear potential $E_0^{tot}(\mathbf{R})$ by means of the Hellmann-Feynman theorem. A *fictitious* classical dynamics over the electronic degrees of freedom will be also allowed in accordance to the Car-Parrinello [1] scheme.

In practice, the many-body terms of (2) make it difficult to be solved, so that it is usually recast in a series of effective single-particle equations:

$$H_{eff}\psi_{\nu_i}(\mathbf{r}_j;\mathbf{R}) = \varepsilon_{\nu_i}\psi_{\nu_i}(\mathbf{r}_j;\mathbf{R}), \tag{6}$$

in which the many-electron wavefunction $\Psi_\mu(\mathbf{r};\mathbf{R})$ in (2) is constructed from the set of the one-electron wavefunctions $\{\psi_{\nu_i}(\mathbf{r}_j;\mathbf{R})\} = \{\psi_{\nu_i}(\mathbf{r}_j)\}$ (the explicit reference to the ionic coordinates will be dropped for simplicity) of (6).

In the Hartree-Fock approximation [3] the many-electron eigenstates in (2) are expressed as a single Slater determinant of the $\{\psi_{\nu_i}(\mathbf{r}_j)\}$. In doing so the effective one-particle operator of (6) is given by:

$$H_{eff}^{HF} = T_{e\ell} + U_{eI} + U_H + U_X. \tag{7}$$

The first two terms of (7) $T_{e\ell}$ and U_{eI} are the electronic kinetic energy and the electron-ion interaction operators. These correspond to the first and third terms of (1) respectively. The electron-electron interaction is described by the integral operators U_H and U_X respectively the Hartree and the exchange operators:

$$U_H\psi_{\nu_i}(\mathbf{r}_i) = e^2 \sum_{j\neq i} \int d\mathbf{r}_j \frac{|\psi_{\nu_j}(\mathbf{r}_j)|^2}{|\mathbf{r}_i - \mathbf{r}_j|}\psi_{\nu_i}(\mathbf{r}_i) \tag{8}$$

and

$$U_X\psi_{\nu_i}(\mathbf{r}_i) = -e^2 \sum_{j} \int d\mathbf{r}_j \frac{\psi^*_{\nu_j}(\mathbf{r}_j)\psi_{\nu_i}(\mathbf{r}_j)\psi_{\nu_j}(\mathbf{r}_i)}{|\mathbf{r}_i - \mathbf{r}_j|}\delta_{\nu_i,\nu_j}. \tag{9}$$

The set of equations (6) represents a non linear eigenvalue problem. It has to be solved iteratively in a self-consistent way.

The total energy expression of the system can be given now as:

$$E_0^{tot} = E_{KE-eI} + E_{ee} + E_{II} \tag{10}$$

In the first term we have grouped together the kinetic energy $T_{e\ell}$ and the electron-ion attraction U_{eI}. Formally it is expressed as

$$E_{KE-eI} = \sum_i \int d\mathbf{r}\psi^*_{\nu_i}(\mathbf{r}) \left[T_{e\ell} + U_{eI}\right] \psi_{\nu_i}(\mathbf{r}) \tag{11}$$

The term E_{ee} is the electron-electron interaction energy. It is the sum of the Hartree energy

$$E_H = \sum_{i<j} \int d\mathbf{r}\psi^*_{\nu_i}(\mathbf{r}) U_H \psi_{\nu_j}(\mathbf{r}) \tag{12}$$

and the exchange energy

$$E_X = \sum_{i<j} \int d\mathbf{r}\psi^*_{\nu_i}(\mathbf{r}) U_X \psi_{\nu_j}(\mathbf{r}) \tag{13}$$

Finally, E_{II} corresponds to the ion-ion repulsion interaction energy given by the last term of (1). All the equations given up to now consider all the electrons in the system. For large systems, however, it becomes prohibitive to treat each

electron explicitly and one can make an approximation: since the valence electrons dominate the interesting physical and chemical properties of the system, only those electrons are explicitly considered as moving in an effective potential that includes all the interactions with the nuclei and the remaining inner electrons. Unless different specified the term *electron* must be understood as *valence electron.*

In the empirical tight-binding methods the electron-electron interactions are not treated explicitly. These interactions are included via the parametrization of the Hamiltonian matrix; that is, the electron-ion and electron-electron terms are "lumped" into a single set of matrix elements. In the evaluation of the total energy in the TB models, the electronic energy is expressed as a sum over the occupied eigenvalues ε_{ν_i} of (6). In the Hartree-Fock approximation this is written as:

$$E_{bs} = \sum_i \varepsilon_{\nu_i} = E_{KE-eI} + 2E_{ee} \tag{14}$$

where the subscript *bs* stands for *band structure.* The band structure energy E_{bs} depends implicitly on $\{\mathbf{R}\}$.

As can be seen from (11-14) the band structure energy E_{bs} overestimates the electronic energy due to double counting of the electron-electron interactions. In methods where the interactions are explicitly computed it is possible to substract the extra terms. In the TB models this extra component of the energy is not explicitly calculated and therefore E_{bs} must be empirically corrected. As first suggested by Chadi [4], the total energy of the system can be written as:

$$E_0^{tot} = E_{bs} + E_{rep}, \tag{15}$$

where

$$E_{rep} = E_{II} - E_{ee}. \tag{16}$$

The term E_{rep} contains the ion-ion and additional electron-electron terms. For two ions that are separated by a distance much larger than the sum of the atomic radii E_{rep} is close to zero. Then a good approximation of this term will be that of a short range potential. E_{rep} can be thought as the sum of two body repulsive potentials $V(R_{kl})$ between all the pairs of nearest–neighbours (NN) ions

$$E_{rep} = \sum_{k<l} V(|\mathbf{R}_k - \mathbf{R}_l|) \tag{17}$$

the explicit form of the $V(R_{kl})$ being something that has to be decided *ad-hoc*. We will come back to this problem later on. The repulsive energy E_{rep} depends explicitly on $\{\mathbf{R}\}$.

In order to find the band structure energy it is assumed that each electron feels a potential due to the ions and to the other electrons, which can be expressed as a sum of *spherical* potentials centered on each ion. The one-electron effective hamiltonian reads :

$$H_{eff}^{TB}(\mathbf{R}) = T_{e\ell} + \sum_{\ell=1}^{N} \mathcal{U}(\mathbf{r} - \mathbf{R}_\ell). \tag{18}$$

The eigenfunctions of (6) are then expressed on a basis of atomic orbitals:

$$\{\phi_\alpha(\mathbf{r} - \mathbf{R}_\ell)\} \tag{19}$$

as

$$\psi_{\nu_i}(\mathbf{r}) = \frac{1}{\sqrt{N}} \sum_{l,\alpha} C_{\nu_i \alpha l} \phi_\alpha(\mathbf{r} - \mathbf{R}_l) \tag{20}$$

where α stands for all the quantum numbers that identify the orbital. This is a key point in the TB methods: it restricts the applicability of the scheme to systems where the electronic charge density is mostly localized around the ions as it happens for example in semiconductors and transition metals. Each orbital (19) satisfies the Schrödinger equation corresponding to the free atom

at which it is centered:

$$\{T_{e\ell} + \mathcal{U}(\mathbf{r} - \mathbf{R}_\ell)\}\, \phi_\alpha(\mathbf{r} - \mathbf{R}_\ell) = \epsilon_\alpha \phi_\alpha(\mathbf{r} - \mathbf{R}_\ell). \tag{21}$$

The eigenvalues ϵ_α are the so called *on-site energy integrals.* In many TB schemes the atomic orbitals $\{\phi_\alpha(\mathbf{r} - \mathbf{R}_\ell)\}$ are supposed to be orthonormal

$$S_{\alpha' l' \alpha l} = \int d\mathbf{r}\, \phi^*_{\alpha'}(\mathbf{r} - \mathbf{R}_{l'}) \phi_\alpha(\mathbf{r} - \mathbf{R}_l) = \delta_{\alpha,\alpha'} \delta_{l,l'} : \tag{22}$$

this will also be our choice. The above orthonormality requirement can always be fullfilled by using the Löwdin [5] orbitals in correspondence to the atomic orbitals of (19). Alternative schemes which use non-orthonormal orbitals are also possible, but we will not discuss them. The one electron eigenvalues of (6) with H_{eff} in the TB approximation (18) are then given by :

$$\varepsilon_{\nu_i} = \int d\mathbf{r}\, \psi^*_{\nu_i}(\mathbf{r}) H^{TB}_{eff} \psi_{\nu_i}(\mathbf{r}) = \frac{1}{N} \sum_{\alpha' l'} \sum_{\alpha l} C^*_{\nu_i \alpha' l'} C_{\nu_i \alpha l} H_{\alpha' l', \alpha l}. \tag{23}$$

with

$$\begin{aligned} H_{\alpha' l', \alpha l} \;=\; & \epsilon_\alpha \delta_{\alpha,\alpha'} \delta_{l,l'} + \\ & (1 - \delta_{l,l'}) \int d\mathbf{r}\, \phi^*_{\alpha'}(\mathbf{r} - \mathbf{R}_{l'}) \mathcal{U}(\mathbf{r} - \mathbf{R}_{l'}) \phi_\alpha(\mathbf{r} - \mathbf{R}_l) + \\ & \sum_{l''} (1 - \delta_{l',l''}) \int d\mathbf{r}\, \phi^*_{\alpha'}(\mathbf{r} - \mathbf{R}_{l'}) \mathcal{U}(\mathbf{r} - \mathbf{R}_{l''}) \phi_\alpha(\mathbf{r} - \mathbf{R}_l). \end{aligned} \tag{24}$$

As can be seen from (24) in the energy overlap integrals $H_{\alpha' l', \alpha l}$ three contributions can be distinguished:

- an *inter-atomic* contribution corresponding to the atomic energies, e.g., on-site energy integrals ϵ_α .
- a *two-center* contribution representing the interaction between two orbitals centered on two different sites mediated by an atomic potential centered at one of the two sites.

- a *three-center* contribution representing the interaction between the orbitals of two different electrons mediated by an atomic potential centered on a third different atom.

An explicit calculation of each $H_{\alpha' l', \alpha l}$ can be carried out in principle. In practice the following series of approximations further simplifies the problem, still retaining its main physical features:

1. Depending on the form of the potential $\mathcal{U}(\mathbf{r} - \mathrm{R}_l)$ and on the radial dependence of the atomic orbitals the sums in (24) can be limited up to a certain distance (i.e. to a certain number of neighbouring atoms) from each atom. We will refer to this truncation as a TB scheme up to n–NN.

2. For each atom, only the atomic orbitals retained to be relevant for a correct description of the physical properties of the system under study are considered. These will usually be the valence shell orbitals (valence basis set). Low-lying excited states might also be needed in addition to the valence ones (extended basis set).

3. Instead of calculate the overlap energies $H_{\alpha' l', \alpha l}$, wich are relevant according to 1.) and 2.), from equation (24) we treat them as tunable parameters to be determined by means of a fitting procedure, in such a way that the most relevant experimental and other *ab initio* theoretical data are correctly reproduced. This approximation, first suggested by Slater and Koster [6] makes the present TB method a semiempirical one.

4. Three-center integrals are ignored because they are systematically smaller than the two-center ones, and much more complicate to obtain. In a self-consistent TB this approximation will be hardly justified but in the

semiempirical approach the choice of the two-center parameters will take them into account in an effective way.

With all these approximations the TB calculation of the band structure term of (15) turns out to be quite simple. In the specific case of Silicon, within the framework of a valence basis semiempirical TB up to first NN we need only **6** parameters: those relative to the sp^3 basis. We have the energies of the $3s$ and $3p$ orbitals, $\langle\epsilon_s\rangle$,$\langle\epsilon_p\rangle$ and the hopping energies $\langle ss\sigma\rangle$, $\langle sp\sigma\rangle$, $\langle pp\sigma\rangle$ $\langle pp\pi\rangle$ corresponding to the interactions between s and p orbitals at the diamond NN distance in the possible principal relative orientations between s and p orbitals [6]. The energy overlap integrals of (24) between two arbitrarily oriented orbitals can be decomposed into the sum of principal orientation contributions by means of simple geometrical rules. The general form of the interactions between two orbitals s or p centered on two first NN with positions $\mathbf{R}_k$ and $\mathbf{R}_{k'}$ is

$$\begin{aligned}
H_{sk,sk} &= \langle\epsilon_s\rangle \\
H_{pk,pk} &= \langle\epsilon_p\rangle \\
H_{\alpha' k,\alpha k} &= 0 \\
H_{sk',sk} &= \langle ss\sigma\rangle \\
H_{sk',pk} &= \langle sp\sigma\rangle\, p_{k'k} = -H_{pk',sk} \\
H_{pk',pk} &= \langle pp\sigma\rangle\, p_{k'k}^2 + \langle pp\pi\rangle\,(1 - p_{k'k}^2) \\
H_{p'k',pk} &= (\langle pp\sigma\rangle - \langle pp\pi\rangle) p'_{k'k} p_{k'k} = H_{pk',p'k}
\end{aligned} \tag{25}$$

where $p_{kk'}$ stands for the direct cosines of the vector $\mathbf{R}_{k'} - \mathbf{R}_k$, with p equal to x, y or z. In the above equations $\alpha \neq \alpha'$, $k \neq k'$ and $p \neq p'$.

We stress that the on-site energies $\langle\epsilon_s\rangle$ and $\langle\epsilon_p\rangle$ differ from the neutral atom values due to the different orbital occupancies in the solids; these occupancies

in turn depend strongly on the particular *environment* of each atom [7].

As mentioned above the values of the TB parameters are determined by fitting some experimental and *ab initio* theoretical data corresponding to a particular crystalline structure.

In silicon for example the values of the hopping energies $\langle ss\sigma \rangle$, $\langle sp\sigma \rangle$, $\langle pp\sigma \rangle$ $\langle pp\pi \rangle$ usually correspond to those of the diamond structure at the NN equilibrium distance R_0. To get into account their dependance on distances $R_{kk'}$ different than R_0, a scaling function

$$f_s = f_s(R_{kk'}) \tag{26}$$

such that $f_s(R_0) = 1$, must be introduced. Then the value of, for example, the $\langle sp\sigma \rangle$ hopping energy at $R_{kk'}$ will be given by $\langle sp\sigma \rangle\, f_s(R_{kk'})$. In general f_s is choosen to be the same for all the different states of coordination and electronic hybridization.

It should be clear from this discussion that there is not a unique TB parametrization: the value and the number of the parameters varies according to the number and species of the atomic orbitals of the basis (19) and also to the order of the NN shell included in the calculation. However, the different set of experimental and *ab initio* theoretical data considered in the fitting will make distinguishable two TB models which are identical from the point of view of the basis orbitals and NN taken into account. We have also to choose a functional form for the two-body short range potential $V(R_{kl})$ and the scaling function f_s.

3 Application to bulk Silicon

Due to its technological importance silicon has been the focus of a very large research activity, both experimental and theoretical. Many structural, vibrational, thermodynamical, electronic, and optical properties of this material are already well known. The reader must not expect new relevant results from the present work: the application of the TB method *(i)* mainly to bulk Si, and —as a first preliminar approach— to *(ii)* some selected surfaces is intended to be an exercise to learn the method, to discuss its applicability to different kinds of problems, and as a starting point for further applications to other more complex systems. In particular the calculations described in the present Section reproduce some work which has already been done and published by other authors.

As explained in the previous section, a valence basis TB model of silicon up to the NN shell, requires **6** tunable parameters, $\langle \epsilon_s \rangle$, $\langle \epsilon_p \rangle$, $\langle ss\sigma \rangle$, $\langle sp\sigma \rangle$, $\langle pp\sigma \rangle$ $\langle pp\pi \rangle$, a two-body repulsive potential, $V(R_{kl})$, and a scaling function f_s. Unless explicitly specified the term *tight–binding parametrization* will refer to all the needed elements for a TB description of a material.

Once the functional form of $V(R_{kl})$ and f_s is conjectured, and the experimental and *ab initio* data to be used in the fit are choosen, the fitting can be carried on. This will be done in a series of steps. Commonly the 6 electronic parameters are obtained first and then those caracterizing the two-body potential and the scaling function. A *good* parametrization is not required to describe perfectly the electronic and structural properties of a single, (e.g. diamond) structure, but rather to describe reasonably well a wide variety of structural geometries caracterized by different bond lenghts and coordinations (this is also called *transferability*). This seems to be partially incompatible

with an accurately modelling of some of the local properties of the diamond silicon structure. Harrison [8] TB parametrization illustrates clearly this point. There the electronic hopping parameters were fitted by requiring that the main free-electron and TB energy bands of the *diamond structure* are equal at the Γ and X points of the Brillouin zone (BZ). The on-site energy parameters $\langle \epsilon_s \rangle$ and $\langle \epsilon_p \rangle$ were taken from Hartree-Fock calculations. The form of Harrison's scaling funcion $f_s(R) \sim R^{-2}$ comes out from the distance dependece of the free-electron eigenvalues. The two-body short range repulsive $V(R)$ potential was determined to scale as R^{-4} using extended Hückel theory results. The proportionality constant V_0 ($V(R) = V_0 R^{-4}$) was determined by fitting the equilibrium lattice parameter of the *diamond structure*. When tested on other silicon crystalline structures the Harrison TB parametrization gives poor results. In particular it overestimates the equilibrium volume of closed packed cubic lattices; it gives the diamond structure more closed–packed than the FCC one. L. Goodwin, A.S. Skinner and D. Pettifor (GSP) [9] were able to correct this deficiencies obtaining a very simple transferable TB parametrization. Other parametrizations [10] are now available, but they will not be discussed in this work.

As just mentioned the very first step is the determination of the 6 electronic parameters $\langle \epsilon_s \rangle$, $\langle \epsilon_p \rangle$, $\langle ss\sigma \rangle$, $\langle sp\sigma \rangle$, $\langle pp\sigma \rangle$ $\langle pp\pi \rangle$. In the GSP parametrization they are essentially those proposed by Harrison [8], the only difference being the on-site terms $\langle \epsilon_s \rangle$, $\langle \epsilon_p \rangle$. This is because, as pointed out in the preceeding section, the on-site term are environment dependent so they must enter the fitting procedure on the step that considers the other structures. In Table (I) the electronic parameters given by Harrison [8], Goodwin [9] and Chadi [4]

Table I: *TB electronic parameters in eV.*

	Parametrization		
	Goodwin	Harrison	Chadi
$\langle \epsilon_s \rangle$	-6.173	-14.79	-5.25
$\langle \epsilon_p \rangle$	2.122	-7.58	1.20
$\langle ss\sigma \rangle$	-1.82	-1.82	-1.94
$\langle sp\sigma \rangle$	1.96	1.96	1.75
$\langle pp\sigma \rangle$	3.06	3.06	3.05
$\langle pp\pi \rangle$	-0.87	-0.87	-1.08

Table II: *Values of the relative equilibrium volumes (REV) for the lattices considered*

	dia	SC	BCC	FCC	β-tin	sh
TB	0.996	0.857	0.775	0.840	0.772	0.817
ab initio	1.011	0.808	0.736	0.735	0.773	0.727

are reported. Chadi's parametrization is included only for comparison, it can be used only nearby the silicon diamond equilibrium structure.

The results for the band structure of Si diamond corresponding to the three different set of electronic parameters of Table (I) are given in Figs. (1.a–c). They are shown together with *ab initio* [11] calculations. Harrison's and GSP's sets of parameters give a better description of the highest valence bands than Chadi's one. On the other hand Chadi parametrization is the only one which gives an indirect gap(1.15 eV), although at the wrong point ($\Gamma \rightarrow L$, rather than $\Gamma \rightarrow X$); experiments give an indirect gap of 1.17eV between X and Γ. Harrison and GSP electronic parameters predict a direct gap at Γ of 1.86 eV and 0.77 eV respectively. Conduction bands are reproduced with a worse accuracy than valence bands. Their description is improved either with a TB up to a higher number of NN or by enlarging the number of atomic orbitals used in the basis, e.g., including Louie peripherial states s^* [12]. This is beyond of the scope of this work.

The transferability of a TB parametrization can be discussed by studying the curves of total energy versus volume for several different structures. Harrison's TB model with a scaling function and two-body repulsive potential

$$\begin{aligned} f_s(R) &= \left(\frac{R_0}{R}\right)^2 \\ V(R) &= V(R_0)\left(\frac{R_0}{R}\right)^4 \end{aligned} \tag{27}$$

(where $R_0 = 2.35$ Å is the equilibrium NN distance in the diamond structure and $V(R_0) = 3.4581\, eV$), as already pointed out, underestimates the equilibrium volume of closed–packed cubic structures. If we denote V^{dia} the equilibrium volume per atom of the diamond structure (whose experimental value is 20.02 $\AA^3$[13]) and as V^x that one of the x structure, the following ordering of the relative equilibrium volumes (REV) is to be expected in accordance to

Figure 1: *(a.): Band Structure obtained with GSP electronic parameters reported on Table (I). Open circles correspond to ab initio calculations [11]*

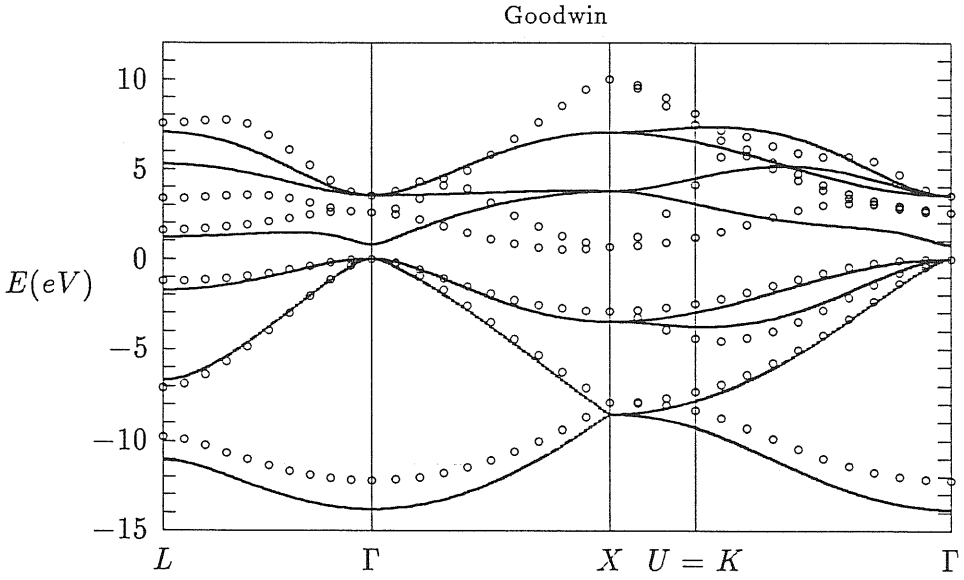

Figure 1: *(b.): Band Structure obtained with Harrison electronic parameters reported on Table (I). Open circles correspond to ab initio calculations [11]*

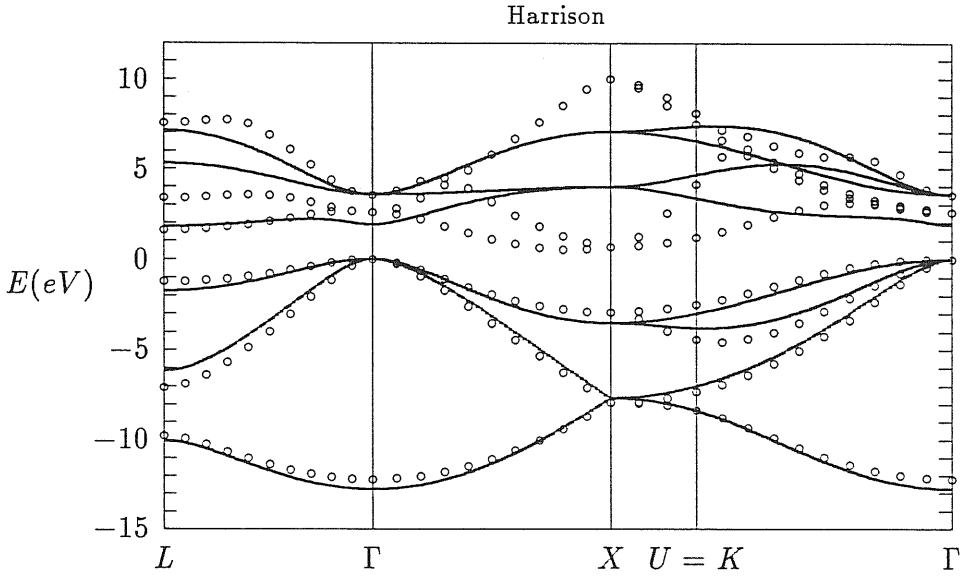

Figure 1: *(c.): Band Structure obtained with Chadi electronic parameters reported on Table (I). Open circles correspond to ab initio calculations [13]*

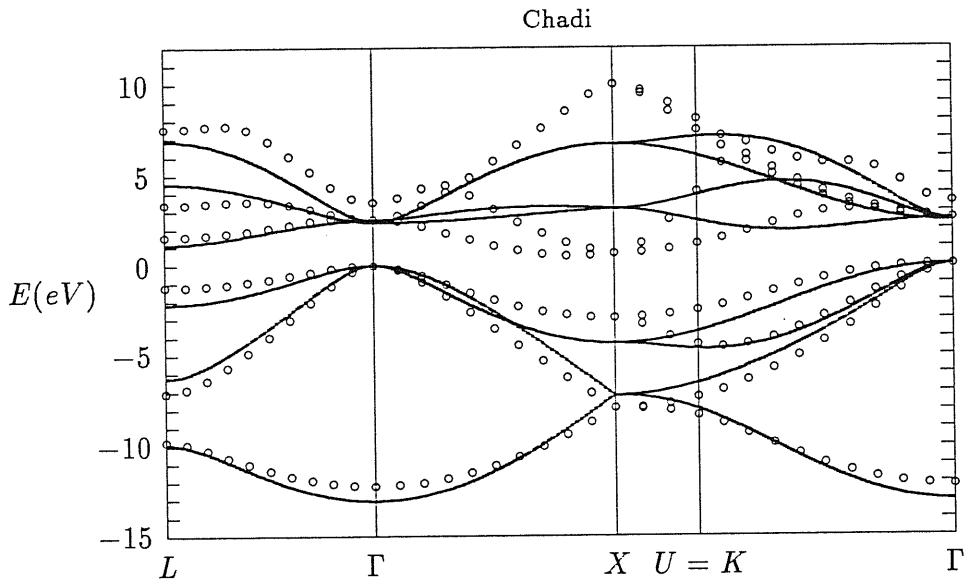

close packing

$$\frac{V^{FCC}}{V^{dia}} < \frac{V^{BCC}}{V^{dia}} < \frac{V^{SC}}{V^{dia}} < 1 \tag{28}$$

In Harrison's scheme the FCC lattice, the most close–packed cubic structure, comes out with an equilibrium volume (EV) per atom larger than that of the diamond structure. This can be seen in Fig. (3.c); figure (3) is the original figure of GSP work.

The cohesive energies E_c are referred to the energy of isolated Si atoms in the ground state electronic configuration $^3P_0$, corresponding to the two p-electrons having the same spin direction according to the Hund's rule. The energy of these spin-polarized configuration is found to be experimentally $0.757eV/atom$ [14] below that of paramagnetic Si(^1D), given by $2(\langle\epsilon_s\rangle + \langle\epsilon_p\rangle)$.

Figure 2: *GSP original figure: in a) are shown ab initio curves of Yin and Cohen [15], in b) those obtained with GSP TB parametrization [9] and in c) those obtained with Harrison TB parametrization [8].*

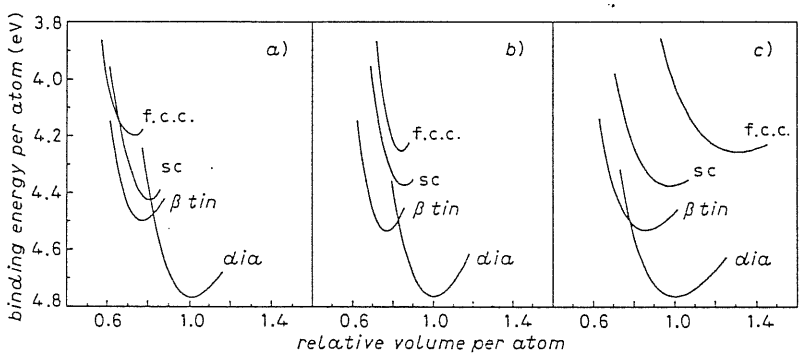

Figure 3: *Curves of cohesive energy per atom(E_c) vs. relative volumes obtained by us with GSP TB parametrization as described in the text. Dots indicate the minimum of Yin and Cohen curves[15].*

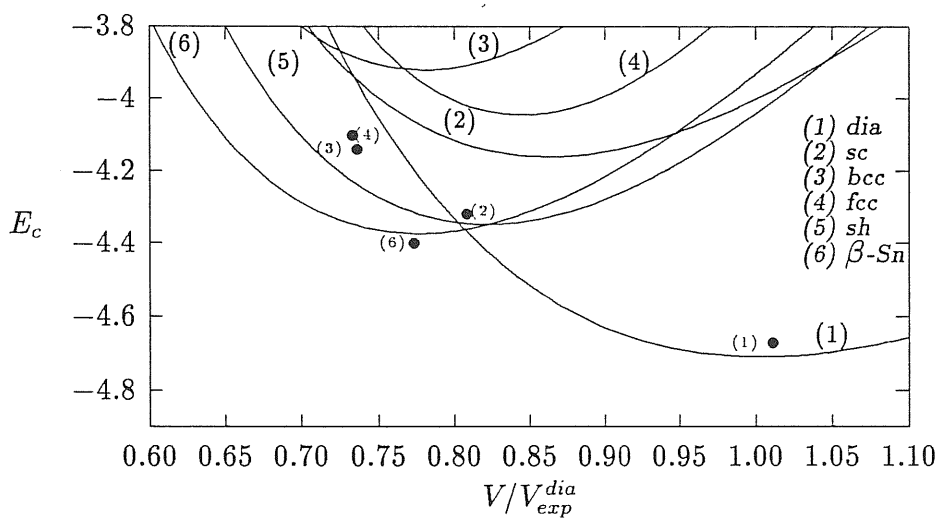

Figure 4: *Harrison[8] and GSP[9] scaling function* $f_s(R)$

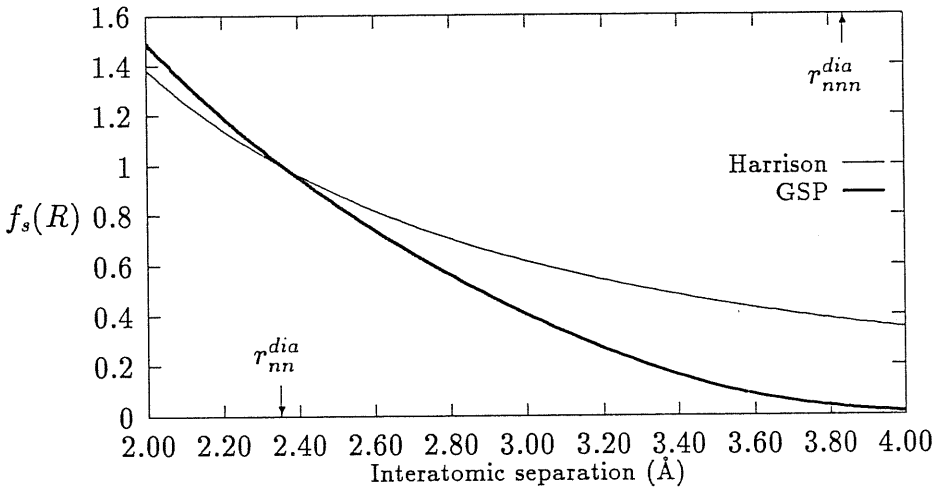

Figure 5: *Harrison[8] and GSP[9] two-body repulsive potential* $V(R)$

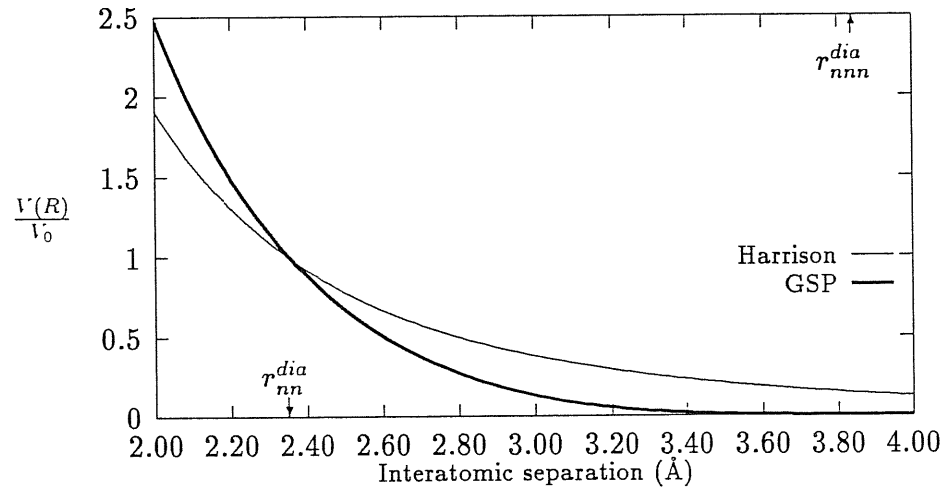

Table III: *Lattice parameters in (Å) and equilibrium cohesive energies E_c in (eV/atom) of several lattices. TB results were obtained by us as described in the text; ab initio data for all the structures except the sh are directly reported from Yin and Cohen (Ref.[15]). Data for the sh indicated with the asterisc were derived by ourselves using Murnagham[18] equation to extract the information from other values reported in Ref.[15].*

lattice		TB	ab initio	Exp.
dia	a	5.424	5.451	5.431
	E_c	-4.71	-4.67	-4.63
SC	a	2.579	2.53	
	E_c	-4.16	-4.32	
BCC	a	3.143	3.09	
	E_c	-3.92	-4.14	
FCC	a	4.066	3.89	
	E_c	-4.04	-4.10	
SH	a	2.733	2.622^*	
	c	2.528	2.444^*	
	E_c	-4.350	-4.608^*	
β-tin	a	4.825	4.828	
	c	2.654	2.655	
	E_c	-4.375	-4.4	

The description of closed–packed cubic structures by Harrison TB parametrization is improved with the use of the GSP scaling function and two body po-

tential

$$
\begin{aligned}
f_s(R) &= \left(\frac{R_0}{R}\right)^n \exp\left[n\left(-\left(\frac{R}{R_c}\right)^{n_c} + \left(\frac{R_0}{R_c}\right)^{n_c}\right)\right] \\
V(R) &= V(R_0)\left(\frac{R_0}{R}\right)^m \exp\left[m\left(-\left(\frac{R}{R_c}\right)^{n_c} + \left(\frac{R_0}{R_c}\right)^{n_c}\right)\right] \qquad (29)
\end{aligned}
$$

where $n = 2$, $m = 4.54$, $r_c = 3.67$ Å, $n_c = 6.48$ and $V(R_0) = V_0 = 3.4581eV$.

We show in Figs. (4) and (5) Harrison and GSP scaling functions and the two-body repulsive potentials. On the figures the diamond nearest and next–nearest–neighbour (NNN) separations are marked. The FCC NNN separation, which is not indicated in the figures, lies close to the diamond NN separation. The figures illustrate the rapid decay of the GSP scaling function f_s and of the two-body repulsive potential $V(R)$ with respect to those of Harrison; it is this rapid decay that allows for a better description of the close packed cubic structures.

In GSP's work the diamond bulk modulus B^{dia}, equilibrium volume V^{dia} and cohesive energy E_c^{dia} were taken from the experimental values, e.g., 0.978 Mbar [13], 20.02 $\mathring{A}^3$ [13] and -4.63 eV/atom [13] respectively; the following parameters

$$m, \Delta\epsilon_{sp}, n_c, r_c \qquad (30)$$

where $\Delta\epsilon_{sp} = \langle\epsilon_s\rangle - \langle\epsilon_p\rangle$, were fitted to the quantities:

$$
\begin{aligned}
\Delta_1 &= E_c^{SC} - E_c^{dia} \\
\Delta_2 &= E_c^{FCC} - E_c^{dia} \\
B^{FCC} & \\
V^{FCC} & \qquad (31)
\end{aligned}
$$

where E_c^{dia}, E_c^{sc} and E_c^{FCC}, are respectively the equilibrium cohesive energies (ECE's) of diamond, simple cubic and fcc phases, B^{FCC} is the FCC bulk modulus and V^{FCC} is the FCC equilibrium volume.

In the curves of Fig.(3.b) and (3.c) for the diamond, simple cubic and FCC lattices only first-neighbour interactions were included in the calculation of the total energy; in that of the β-tin lattice also second–NN were.

We decided to test the applicability of GSP TB parametrization on other crystal structures than those reported in Goodwin's work. In particular, we were interested in the simple hexagonal and BCC lattices. Our results are presented in Tables (III), (II) and Fig. (3); we also include in our calculations the lattices already studied. In all the structures but β-tin and simple hexagonal only first-neighbour interactions were included in the calculation of the total energy; for β-tin and simple hexagonal also second-neighbours were. To calculate the band structure energy (14) we perform BZ integrations using the special point technique suggested by H.J. Monkhorst and J.D. Pack [16] with the Gaussian-smearing method [17] for metallic structures. The curves of Fig.(3) were obtained by a least-squares-fit to Murnagham's equation of state [18].

The present energy-volume curves are different from the published ones of Fig.(3). There is a *sistematic* shift of about 0.2 eV in the ECE, our curves lying above GSP's ones. Since we include the same nearest and next-nearest neighbour interactions than those reported by GSP, the difference on the curves may probably lie in the different method for calculating the band-structure energy. GSP used the recursion method (ref.[5] of GSP work).

The cubic structures are well described, even though condition (28) is not fully satisfied as can be seen from Table(II). The errors in the ECE and REV are within the 10%. For the diamond structure the results were compared with the experimental data of [13] for the REV's and to that of ref.[32] of Yin and Cohen for the ECE's. For the FCC, BCC and SC structures all the data were compared with the *ab initio* results of [15]. The only quantity that from

calculations turns out with an error above the 10%, i.e. $\approx$ 15%, is paradoxically one of the inputs of the GSP fit: the relative equilibrium volume of the FCC lattice. This can be attributed again to the difference in the methods used for calculating the band-structure energy. The results for the REV's and ECE's of the β-tin are in very good agreement with *ab initio* values.

4 The Molecular Dynamics scheme

Classical molecular dynamics simulations has been attracting a lot of interest due to their powerful capability of studying systems at finite temperature, in the investigation of kinetics in various processes, as well as in locating the ground state of complex systems with many degrees of freedom. However, the application of the method to real systems is limited by our knowledge of the interaction potentials or forces acting among the atoms.

No conventional pair potential can stabilize the tetrahedral structure because pair potentials fail to represent the strong electronic covalent binding effects present in such a structure. It is indeed possible to achieve it with the use of complicated forms for the interaction potential. However, such potentials cannot describe satisfactorily *all* the different states of coordination and electronic hybidization of Si [19].

On the other hand, much progress has been made during the past decade in the calculation of various structural and vibrational properties of solids, in a fundamental first-principles approach with the use of density-functional calculations. However, such calculations were almost always limited to considerations of zero-temperature systems. The investigation of disorder and temperature effects is still a difficult problem.

Recently, R. Car and M. Parrinello [1] proposed a scheme which unifies the approaches of density functional theory and molecular dynamics and allows a quantum-mechanical calculation of the interatomic forces. This scheme is, in principle, fundamental and superior to any other proposed approach. However, in practice it requires so much computational effort that, at present, it is restricted to rather short simulation times, of the order of a picosecond, and small number of atoms, few hundreds at most on the most powerful parallel

machines available today.

To handle with the limitations of the Car-Parrinello scheme a simplified one has been proposed [20] which tries to overcome the difficulties in the fully *ab initio* approach by calculating the electronic energies and Hellman-Feynman forces by an empirical TB method like the one described in the first section. It is called the Empirical Tight-Binding Molecular Dynamics (ETBMD) method. In what follows we will describe some general features of the Car-Parrinello scheme; the specific details regarding the ETBMD method will be discussed later on.

The Car-Parrinello scheme

The underlying idea of the Car-Parrinello scheme is that a fictitious dynamics is introduced for the electronic wave functions. This fictitious dynamics is treated in the same manner as the dynamics of the atoms by integrating Newton-type equations of motions. The *classical dynamical* evolution of the electronic and ionic variables is generated by the Lagrangian:

$$\begin{aligned} \mathcal{L}\left(\{\mathbf{R}_\ell\},\left\{\dot{\mathbf{R}}_\ell\right\},\{\psi_i(\mathbf{r})\},\left\{\dot{\psi}_i(\mathbf{r})\right\}\right) &= \frac{1}{2}\mu\sum_{i=1}^{n_s}\int\left|\dot{\psi}_i(\mathbf{r})\right|^2 d\mathbf{r} + \\ \frac{1}{2}\sum_{\ell=1}^{N} M_\ell\dot{R}_\ell^2 - E_0^{tot}\left(\{\mathbf{R}_\ell\},\{\psi_i(\mathbf{r})\}\right) &+ \sum_{i,j}\Lambda_{ij}\left(\int\psi_i^*(\mathbf{r})\psi_j(\mathbf{r})d\mathbf{r}-\delta_{ij}\right), \end{aligned} \tag{32}$$

where the electronic wave-functions $\psi_i(\mathbf{r}) = \langle\mathbf{r}|\psi_i\rangle$ are regarded as classical fields, M_ℓ are the ionic masses, E_0^{tot} is the total energy functional, μ is a masslike parameter with dimensions of an energy times a squared time, and the last term ensures orthonormality of the wave-functions.

The equations of motion resulting from the Lagrangian (32) are:

$$\begin{aligned} \mu\ddot{\psi}_i(\mathbf{r},t) &= -\frac{\delta E_0^{tot}}{\delta\psi_i^*(\mathbf{r})} + \sum_j\Lambda_{ij}\psi_j(\mathbf{r}) \\ M_\ell\ddot{\mathbf{R}}_\ell &= -\frac{\partial E_0^{tot}}{\partial\mathbf{R}_\ell} = \mathbf{F}_\ell, \end{aligned} \tag{33}$$

and

$$N_{ij}(t) = \int \psi_i^*(\mathbf{r},t)\psi_j(\mathbf{r},t)d\mathbf{r} = \delta_{ij}. \tag{34}$$

From Eqns.(32) and (33) the unknowns $\psi_i(\mathbf{r},t)$, $\mathbf{R}_\ell(t)$, and $\Lambda_{ij}(t)$ can be obtained for any choice of the initial conditions $\mathbf{R}_\ell(0)$,$\dot{\mathbf{R}}_\ell(0)$, $\psi_i(\mathbf{r},0)$, $\dot{\psi}_i(\mathbf{r},0)$ such that $N_{ij}(0) = \delta_{ij}$ and $\dot{N}_{ij}(0) = \delta_{ij}$.

The Parrinello-Blöchl solution of the adiabaticity problem

The dynamics generated by the Car-Parrinello Lagrangian (32) is meaningful only if the electrons are in the ground state for each instantaneous ionic configuration, i.e. they stay on the Born-Oppenheimer surface. This implies that the two subsystems, electronic wave functions $\{\psi_i(\mathbf{r})\}$ and ions must not be in thermal equilibrium; the temperature related to the electronic wave functions must be very low compared with the physically relevant temperature of the atomic subsystem. However, the tendency of the system is to transfer energy between the electronic and ionic degrees of freedom and equilibrate the temperatures of the two subsystems. In this way the electronic wave-functions tend to heat up and leave the Born-Oppenheimer surface, accompanied by a cooling of the atomic systems. For non metals the classical adiabatic approximation is enough for the electons to be always in the Born-Oppenheimer surface. For metals it is not. The problem was solved by Blöchl and Parrinello [21] combining two Nosé [22] thermostats to the Car and Parrinello method of (32). The equations of motion in the Parrinello-Blöchl scheme corresponding to those of (33) are given by

$$\begin{aligned} \mu\ddot{\psi}_i(\mathbf{r},t) &= -\frac{\delta E_0^{tot}}{\delta\psi_i^*(\mathbf{r})} + \sum_j \Lambda_{ij}\psi_j(\mathbf{r}) - \ddot{\psi}_i(\mathbf{r},t)\dot{x}_e\mu \\ M_\ell\ddot{\mathbf{R}}_\ell &= \mathbf{F}_\ell - M_\ell\dot{\mathbf{R}}_\ell\dot{x}_R = \mathcal{F}_\ell \end{aligned} \tag{35}$$

We will denote as $\mathbf{F}_\ell$ the Hellman-Feynman forces and as $\mathcal{F}_\ell$ the forces acting

on the atoms in the simulation. In general they are different because of the inclusion of extra degrees of freedom such as Nosé thermostats or, as will be illustrated in what follows, simulation-box dynamics. The last term of equation (35) is a friction term which couples electronic wave function and ionic dynamics to the Nosé thermostats. These friction terms are governed by the dynamical variables x_e and x_R, which obey the following equations of motion:

$$\begin{aligned} Q_e \ddot{x}_e &= 2\left[\sum_i \mu \int \left|\dot{\psi}_i(\mathbf{r})\right|^2 d\mathbf{r} - E_{kin,0}\right] \\ Q_R \ddot{x}_R &= 2\left[\sum_i \frac{1}{2} M_\ell \dot{\mathbf{R}}_\ell^2 - \frac{1}{2} g k_B T\right] \end{aligned} \tag{36}$$

The fictitious kinetic energy of the electronic wave functions fluctuates about the mean value $E_{kin,0}$ and the average kinetic energy of the ions is $\frac{1}{2} g k_B T$, where g is the number of degrees of freedom for the atomic motion, k_B is the Boltzmann constant, and T is the physical temperature of the simulation. The masses Q_e and Q_R determine the time scales for the thermal fluctuations.

A proper choice of the value of $E_{kin,0}$ is very important for a physically relevant simulation: if, on one hand, this value is too large, the electronic wave functions will depart from the Born-Oppenheimer surface and eventually become meaningless. If, on the other hand, it is too small, the electrons cannot easily follow the atomic motion, which results in a delay of the ionic motion. In Ref. [21] are given some clues about the adequate choice of $E_{kin,0}$.

The Parrinello-Rahman scheme for phase transition simulations

A pressure driven phase transition of a solid can be studied on a computer simulation only if the volume and possibly also the shape of the simulation box are allowed to change during the simulation; this simulation box properties are to be considered as dynamical variables. It was first proposed, within the framework of classical molecular dynamics, a coupling of the system to

an external variable V, the volume of the simulation box[23]. This coupling mimics the action of a piston on a real system. Best suited for solid state simulations is to allow the simulation box also to change in shape; this is what was done by Parrinello and Rahman[24] work also in the framework of classical molecular dynamics. Generalized to the Car-Parrinello scheme of (32) the Parrinello-Rahman approach leads to the following equations of motion[25]:

$$\begin{aligned} \mu\ddot{\psi}_i(\mathbf{s},t) &= -\frac{\delta E_0^{tot}}{\delta\psi_i^*(\mathbf{s})} + \sum_j \Lambda_{ij}\psi_j(\mathbf{s}) \\ M_\ell\ddot{\mathbf{S}}_\ell^\alpha &= -\frac{\partial E_0^{tot}}{\partial \mathbf{R}_\ell^\beta}(\mathbf{h}^t)^{-1}_{\beta\alpha} - \mathcal{G}^{-1}_{\alpha\beta}\dot{\mathcal{G}}_{\beta\gamma}\dot{\mathbf{S}}_\ell^\gamma = \mathcal{F}_\ell^\alpha \end{aligned} \tag{37}$$

where $\mathbf{r} = \mathbf{hs}$, $\mathbf{R} = \mathbf{hS}$ with

$$\mathbf{h} = (\mathbf{a}, \mathbf{b}, \mathbf{c}) \tag{38}$$

is the matrix made up with the three primitive Bravais vectors $(\mathbf{a}, \mathbf{b}, \mathbf{c})$ where the vectors constitute its columns. The metric tensor $\mathcal{G} = \mathbf{h}^t\mathbf{h}$ gives the relation between the distances in real, e.g. R, and scaled, e.g. S, coordinates. The dynamics of the box will be given by:

$$W\ddot{\mathbf{h}}_{\alpha\beta} = (\Pi_{\alpha\gamma} - p\delta_{\alpha\gamma})\,\Omega(\mathbf{h}^t)^{-1}_{\gamma\beta} \tag{39}$$

In the above equation $\Omega = det(\mathbf{h})$ is the instantaneous volume of the simulation box, W is the box mass, p is the external pressure and Π is the internal stress tensor. We will come back to this considerations in the next section where the problem of the single dimer geometry in the ground state configuration of the reconstructed Si(100) surface will be faced. There we will allow also for a dynamics of the simulation box according to (39).

The ETBMD scheme

Originally in the Car-Parrinello scheme the electronic contribution to the total energy E_0^{tot} in (32) was calculated within the local-density-functional approximation with a plane-wave basis set. A parametrized TB approach to

calculate the total energy (see (15)) reduces drastically the computation time. It was estimated that a TB code runs about a factor of 20 faster than the corresponding density-functional version [20]; the compromise between computational speed and accuracy of the ETBMD scheme is considered satisfactory.

As stated before in the TB approximation a minimal basis set like that of (19) is used, consisting only of those orbitals which are occupied or partially occupied in the free atom; the matrix elements of the Hamiltonian are treated as tunable parameters. The electronic wave functions $\psi_i(\mathbf{r},t)$ are expanded in the localized basis functions of (19) as :

$$\psi_i(\mathbf{r},t) = \frac{1}{\sqrt{N}} \sum_{\ell,\alpha} C_{i\alpha\ell}(t)\phi_\alpha(\mathbf{r}-\mathbf{R}_\ell). \tag{40}$$

In this way the dynamics of the electronic degrees of freedom will be in terms of the coefficients $\{C_{i\alpha\ell}(t)\}$ of expansion (40) insted of the wave-functions $\psi_i(\mathbf{r},t)$. For example, equations (33) and (34) are written in terms of the expansion coefficients as:

$$\begin{aligned} \mu\ddot{C}_{im}(t) &= -\frac{\delta E_0^{tot}}{\delta C_{im}^*} + \sum_j \Lambda_{ij} C_{jm} \\ M_\ell \ddot{\mathbf{R}}_\ell &= -\frac{\partial E_0^{tot}}{\partial \mathbf{R}_\ell} = \mathbf{F}_\ell \end{aligned} \tag{41}$$

and

$$N_{ij}(t) = \sum_m C_{im}^*(t) C_{jm}(t) = \delta_{ij} \tag{42}$$

where the index m stays for (i,α).

The 'velocity Verlet' algorithm for numerical integration

In practice the equations of motion for ions and electrons are integrated numerically. In the calculations performed in the next section we use for this purpose the 'velocity Verlet' algorithm[26], which for the ionic coordinates takes

the following form

$$\begin{aligned} \mathrm{R}_\ell(t+\Delta t) &= \mathrm{R}_\ell(t) + \mathrm{V}_\ell(t) + \frac{\Delta t^2}{2M_\ell}\,\mathcal{F}_\ell \\ \mathrm{V}_\ell(t+\Delta t) &= \mathrm{V}_\ell + \frac{\Delta t}{2M_\ell}\,[\,\mathcal{F}_\ell\,(t) + \,\mathcal{F}_\ell\,(t+\Delta t)] \end{aligned} \tag{43}$$

An analogous of the above equation holds also for the coefficients C_{im}. The dynamics for the electrons is usually performed only on the coordinates belonging to the occupied subspace of the electronic eigenvectors; the vectors of the unoccupied subspace do not enter. We also adopt this scheme for our simulations.

5 Application to Silicon surfaces

In section 2 we studied the applicability of the GSP TB parametrization to bulk silicon. The equilibrium volumes and cohesive energies for a series of structures were calculated, the results showing satisfactory agreement with *ab initio* calculations; a more demanding test for a TB parametrization comes from the study of surface reconstructions. We will focus in what follows on the Si(100) clean surface reconstruction.

A truncated 1x1 Si(100) surface, Fig. (6.a), contains two unsaturated or dangling bonds per atom; the system tends to minimize its energy by reconstructing its surface. Theoretical [27] and experimental [28,29] evidence shows that this reconstruction is accompained by the creation of dimers; i.e., surface atoms move toward each other as indicated on Figure (6.b). Furthermore, these dimers are tilted and asymmetric (Fig. 6.c). The tilting is accompanied by an electronic charge transfer from the lower to the upper atom of the dimer. In addition to that, the dimers can arrange themselves in various patterns on the surface with different supercells and thus many reconstructions of the surface

are possible. In Figure (6.c, .d, .e) we show a few important reconstructions for the Si(100) surface, the (2x1), p(2x2) and c(4x2) respectively.

The calculated energy difference per surface atom between the bulk truncated surface and the (2x1) symmetric dimers reconstructed surface(Fig.(6.b)) is in the range 0.5-0.8 eV [27], the appearance of dimers lowering the energy. Tilting of dimers further lowers the energy. The (2x1) tilted dimers reconstructed surface(Fig.(6.c)) has an energy of about 0.05 eV per surface atom lower than the (2x1) symmetric dimers reconstructed surface.

The relative stability between the (2x1) and other high-order reconstructions, such as p(2x2) and c(4x2), represents a difficult problem since the energy differences among the different reconstructions are of the order of few tenths of meV per surface atom [27]. The smallness of this energy differences is due to the fact that dimers are weakly interacting one with each other [30]. Instead of trying to establish the relative stability between a series of candidate tilted dimers reconstructions in what follows we will focus on the study of single dimer properties.

5.1 Si(100) surface reconstruction: single dimer properties

In order to simulate the Si(100) surface we consider a slab of eight silicon layers with 16 atoms per layer (128 atoms in total). Top and bottom layers correspond to the two surface layers. We indicate with (xy) the planes parallel to the surfaces, and z is the perpendicular direction. Periodic boundary conditions are applied in the (xy) planes to simulate an infinitely extended surface. We will label the layers as 1,2,3, ... ,8 from the bottom to the top.

Surface dimerization causes sizeble elastic distortions of deep layers [31].

In our simulation cell layers 4 and 5 should retain bulk properties. To study individual dimer properties it will be in principle sufficient a slab with just one (2x1) unit surface cell. On the other hand a larger size of the simulation cell is required for a proper calculation of the band structure term, since only the Γ point is used in sampling the Brillouin zone. We obtain a reasonable convergence without too much computational effort with 16 atoms per layer. This cell size allows for surface periodicities up to 4x4. The bulk NN equilibrium distance used was 5.424 Å.

The surface formation energy is defined as the energy needed to create a surface from the bulk. Our TB calculation gives that to create an ideal unreconstructed clean 1x1 Si(100) surface 1.61 eV/surf.atom are needed.

The 'dynamical quench' procedure used proceeds along the following steps:

- Start with the ions at a temperature of 300 ° K degrees.
- Start a Car-Parrinello dynamics without external pressure but allowing also for box dynamics.
- *Quench over the ionic degrees of freedom*: every time that

$$\sum_{\ell} \mathbf{v}_{\ell} \, \mathcal{F}_{\ell} \; < 0 \tag{44}$$

  then

$$\mathbf{v}_{\ell} = 0, \forall \ell \tag{45}$$

- *Quench over the box degrees of freedom*: the same as above.
- We stop when the change in the total energy of the system ε_0^{tot} was less than $10^{-4} eV/atom$ over the last few hundred steps of the simulation.

All over the quench we have a thermostat like that of (35) and (36) acting on the electrons. The thermostat on the ions is off. The values of the simulation parameters used in all our calculations are shown in Table (IV).

The starting point for the first calculation was the ideal unreconstructed 1x1 surface. Only for this calculation in addition to heating the ions we randomly displaced them by about 0.1Å. After 3500 quenching steps we didn't find any evidence of dimers on the surfaces, the surfaces looking similar to the ideal unreconstructed one. The energy gain results to be of -0.04 eV/surface atom coming mainly from ionic relaxation along the z direction. In Table(V) we report the average interlayer distances of the upper half of the slab, the lower being almost identical; bulk interlayer distance is also reported for comparison.

We decided then to start from a surface configuration with the dimers already formed. From the slab with the two ideal unrecontructed 1x1 surfaces we move 'by hand' only the upper and lower surface atoms (all the other atoms were kept at the ideal bulk positions) in order to get *symmetric* dimers. We kept all bond lengths fixed. In few words we start from a 2x1 symmetric dimers reconstructed surface like that of Figure(6.b). A 3D view of the upper half of our simulation cell is shown in Figure(7). The energy difference of this symmetric dimers configuration with respect to the ideal unreconstructed 1x1 surface was found to be 0.05 eV, the 'reconstructed' configuration lying above the ideal one. This result seems to disagree with the well established fact that surface dimerization is energetically favoured. However, as stated before, surface dimerization causes also sizeble elastic distortions of deep layers, distortions not allowed in our present configuration. This explains why we get a *positive* energy gain.

After 3000 steps of quench we got that *all* the dimers on both surfaces were tilted, the energy gain of this final configuration being of -0.44 eV/surf.atom. A

Figure 6: *Schematic indication of : (a) top view and side view of the ideal (truncated bulk) Si(100); top view and side view of the symmetric (b) and asymmetric (c) dimer 2x1 reconstructions; top view of the p(2x2) (d) and c(4x2) (e) asymmetric dimer reconstructions.*

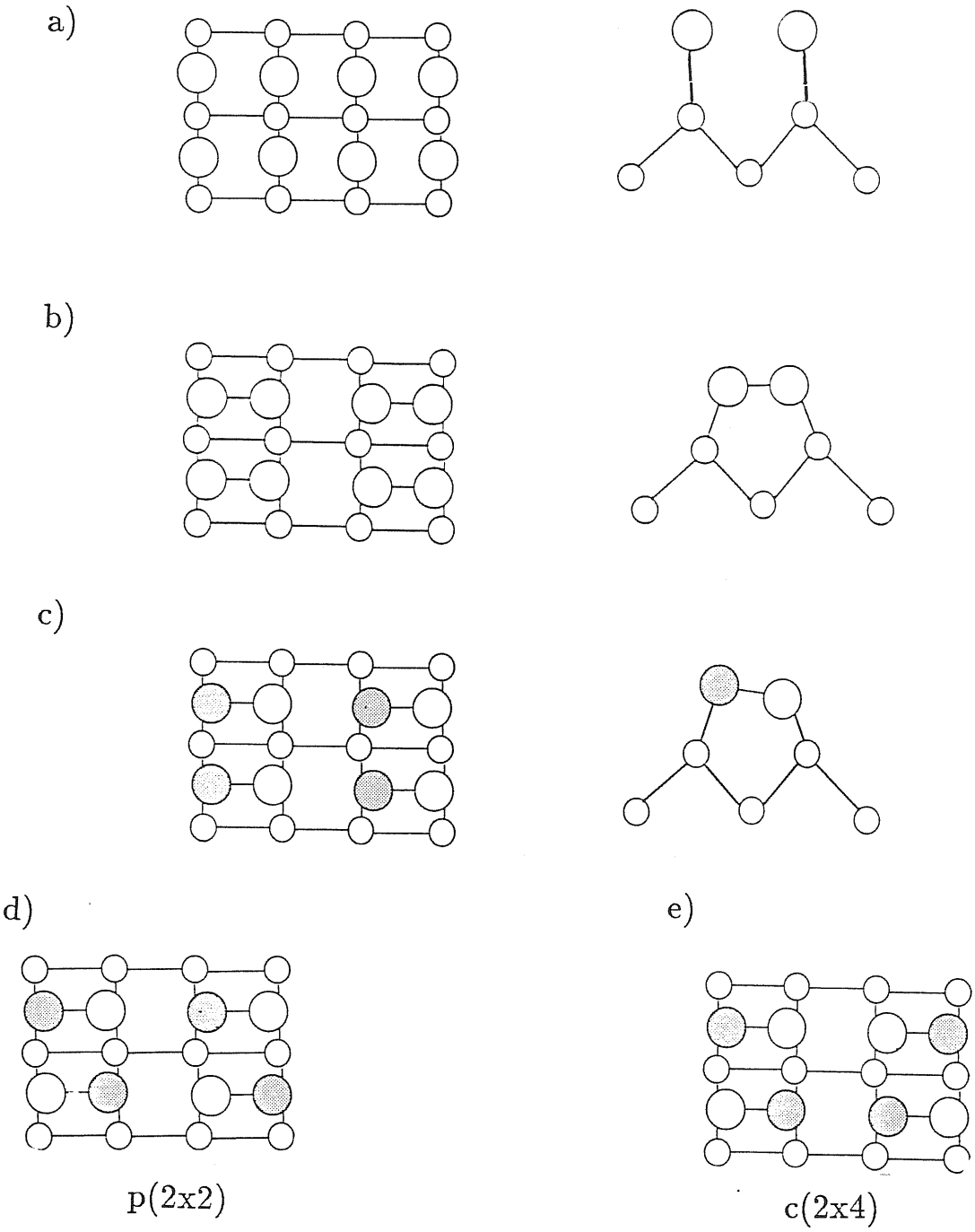

3D view of all the slab is shown in Figure(8); 3D and top-view(upper surface) of the upper half are shown in Figures(9.a,.b), for the lower half these are shown on Figures(10.a,.b).

As expected from what stated in the introductory remarks the tilting of the dimers is energetically favorable. Although the periodicity of the dimer reconstruction of the two surfaces is different the configuration of the dimers are very similar. Single dimer configuration is illustrated on Figure (11), and the relevant characteristic quantities (lengths, angles, charge transfers) are reported on Table(VI). The charge transfer δq is defined as

$$\delta q = \frac{q_1 - q_2}{2} \tag{46}$$

where q_1 and q_2 indicate the charge (in units of the electron charge) of the upper and lower atoms of the dimer(see Fig. (11)).

Our results are in reasonable agreement with those of other theoretical calculations. The values of the tilting angle θ, the difference dz of the z coordinates of the two atoms of the dimer and the bond-lenght r_{12} are in good agreement with those obtained from density-functional-theory calculations ([30],[32]). Other TB molecular-dynamics studies ([20]) give also results close to ours. Chadi's results ([4],[33]) are in reasonable agreement with ours.

It is difficult to determine the single-dimer properties from experiments. It can be done for example by LEED experiments in an indirect way. The experimental variation of scattered beam intensity against incident energy is compared with that obtained by an elaborated calculation. The coordinates of the surface and subsurface atoms are determined by fitting the experimental intesity profiles with those obtained by the calculations. In Table (VI) we report one of these LEED-fitting results ([28], Yang, Jona and Marcus work). It can be seen that the only quantity in good agreement with our calculation

is the dimer bond-lenght r_{12}. For θ and dz the error is of the order of 50 %. However the LEED values were obtained by fitting the experimental data to an assumed 2x1 tilted dimer reconstructed surface. It is well established from STM experiments [29] that the samples exhibit a complex geometry, i.e. they show coexistence of symmetric and asymmetric dimer domains, as well as dimer vacancies. Taking this into account the values for θ and dz of Table (VI) coming from LEED experiments must be interpreted as *mean value* results, that is as an average over symmetric and asymmetric dimers domains. All the above mentioned experiments were carried on at finite temperatures, the lowest reported being 120° K ([29]) while our calculation corresponds to the ground state, i.e. T=0° K, configuration. In Wolkow's work it was directly observed that the cooling up to 120° K is accompained by an increasing of the number of buckled, i.e. twisted, dimers and conversely by a reduction of symmetric dimers.

The distances between the atoms belonging to two adjacent dimers are all longer than the NNN distance for bulk silicon ($\sim$ 3.8 Å); at this internuclear distance the two-body repulsive potential $V(R)$ and the scaling function $f_s(R)$ are almost negligible, resulting in a weak coupling of the dimers. This weak coupling between the dimers is however confirmed by other theoretical results[30].

We can therefore conclude that GSP parametrization gives reasonable results also when applied to the problem of the reconstruction of the Si(100) surface, supporting the well established experimental and theoretical evidence of tilted dimers as the building block of the reconstruction.

Table IV: *Simulation parameters*

Parameter	Value	Units
Δt	$1.62\text{x}10^{-14}$	s
μ	0.01	eV x s^2
M_ℓ	$4.67\text{x}10^{-23}$	g
Q_e	$1.16\text{x}10^{-31}$	eV x s^2
W	$2.32\text{x}10^{-22}$	g
$E_{kin,0}$	$1\text{x}10^{-3}$	eV/electron state
g	3	

Table V: *Interlayer distances in Å*

$8 \leftrightarrow 7$	$7 \leftrightarrow 6$	$6 \leftrightarrow 5$	$5 \leftrightarrow 4$	**bulk**
1.443	1.401	1.384	1.376	1.356

Figure 7: *Symmetric dimers initial configuration, 3D view*

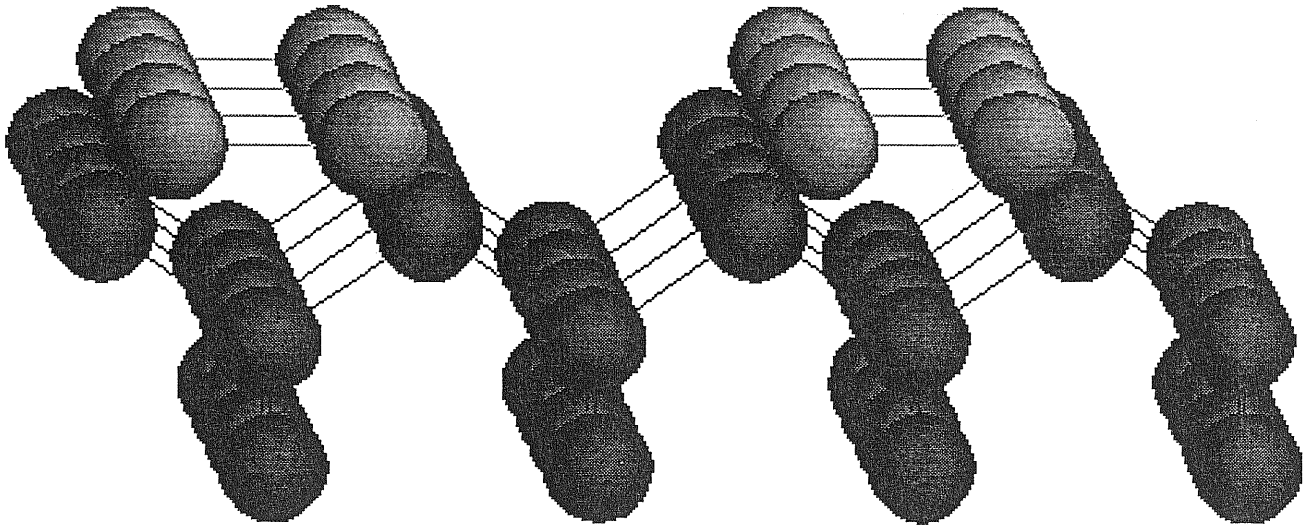

Figure 8: *Total slab after the quench, 3D view*

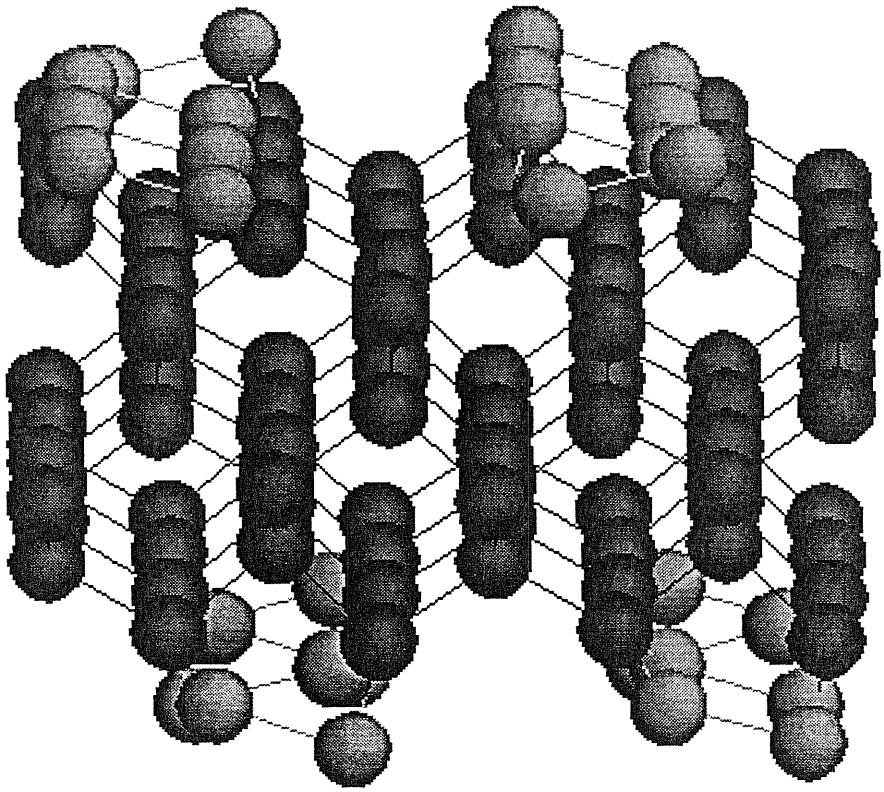

Figure 9: *Upper half after the quench: 3D and top(upper surface) views*

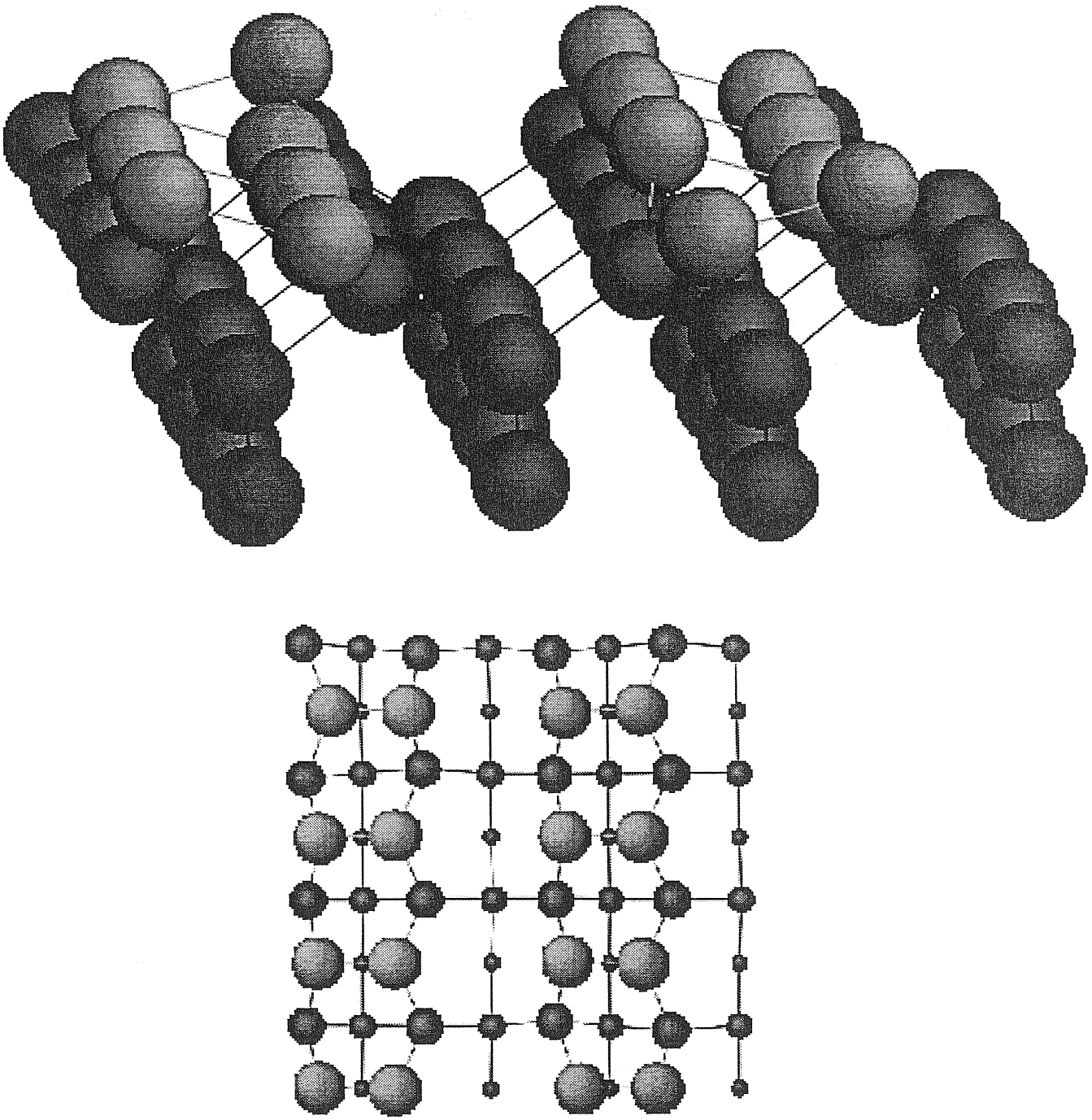

Figure 10: *Lower half after the quench: 3D and top(lower surface) views*

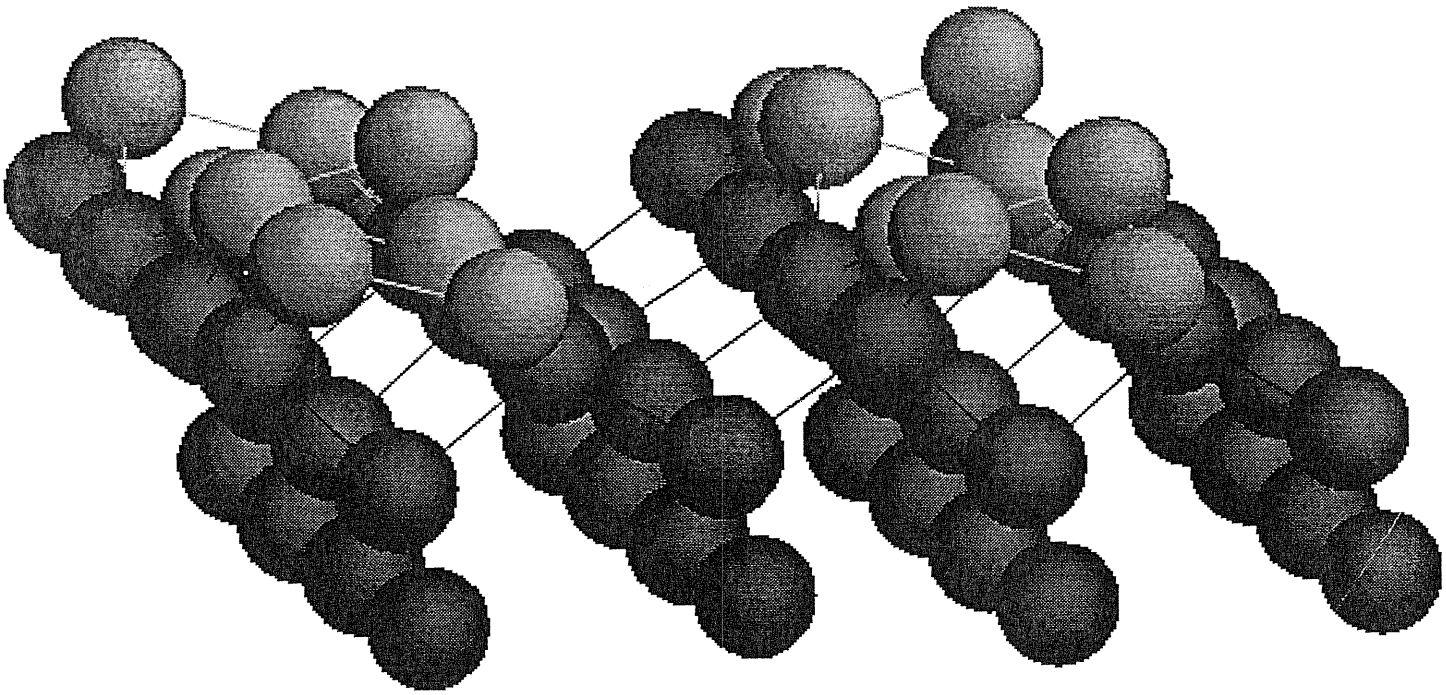

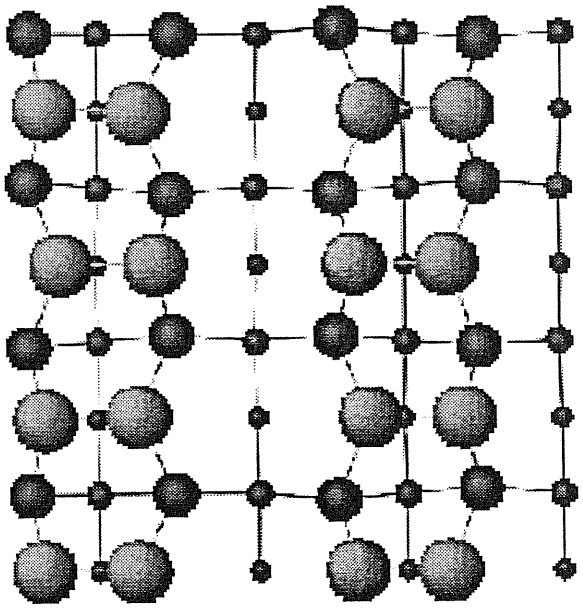

Figure 11: *A single dimer*

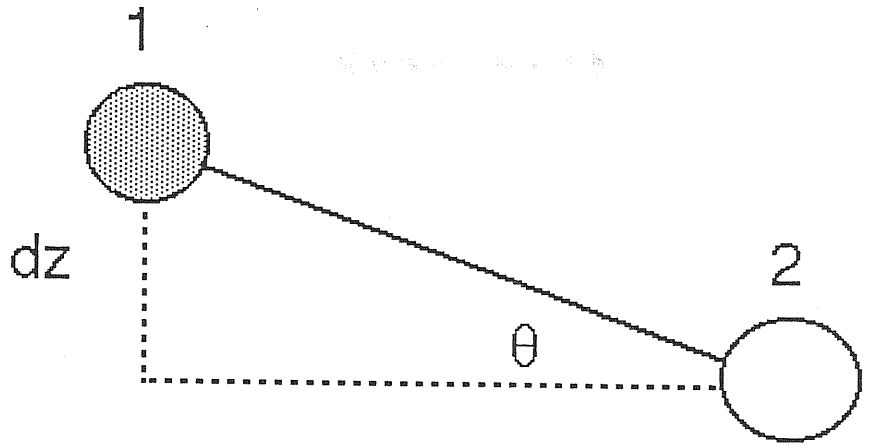

Table VI: *Single Dimer Properties*

	θ	δq	dz(Å)	r_{12}(Å)
This work	16°±1.04°	0.32±0.02	0.67±0.04	2.42±0.005
Ref.[30]	15°			
Ref.[27]	11°	0.45	0.45	2.35
Ref.[33]	11°	0.36	0.43	2.35
Ref.[20]		0.39	0.59	
Ref.[32]	13°		0.69	2.29
Ref.[28]	8.5°±1°		0.364±0.05	2.47±0.3

6 Conclusions

A preliminar work based on the Empirical Tight-Binding Molecular Dynamics(ETBMD) scheme has been presented here, aimed basically at learning the method and discussing its applicability to different kinds of problems. We choose to study silicon, being the focus of a very large experimental and theoretical research activity. Among the various TB parametrization available in the literature we chose the one proposed by Goodwin, Skinner and Pettifor [9] which turns out to be simple but accurate enough.

After a general discussion about Empirical TB methods we studied the transferability of the parametrization considered. The curves of cohesive energy *versus* volume were computed for several lattices; to this purpose we implemented a FORTRAN code which can be used for further applications to other more complex systems. The curves above mentioned were in reasonable agreement with those from *ab initio* calculations.

We tested the Empirical TB method by studying the Si(100) clean surface reconstruction. Our results provide further evidence of tilted dimers as the building block of the reconstruction. The single dimer geometry was in accordance to that obtained from other ETBMD simulations and *ab initio* calculations. The study of surface reconstruction requires quite large simulation cells. We carried on our simulation with a 128 atoms cell with a non parallel ETBMD code on an IBM Risc 6000/580 machine.

References

[1] R. Car and M. Parrinello, Phys.Rev.Lett. **55**, 2471 (1985).

[2] M. Born and J.R. Oppenheimer, Ann.Phys. **84**, 457(1927).

[3] B.H. Bransden, *Physics of atoms and molecules*, (Longman Scientific, Hong Kong, 1983).

[4] D.J. Chadi, Phys.Rev.Lett. **41**, 1062(1978).

[5] P.O. Löwdin, Jnal.Chem.Phys. **18**, 365(1950).

[6] J.C. Slater and G.F. Koster, Phys.Rev. **94**, 1498(1954).

[7] for more details about this see J.A. Majewski and P. Vogl, *The Structures of Binary Compounds* edited by F.R. de Boer and D.G. Pettifor, (Elsevier,1989) and references therein.

[8] W.A. Harrison, *Electronic Structure and the Properties of Solids*, (Freeman, New York, 1965) and references therein.

[9] L. Goodwin, A.J. Skinner and D.G. Pettifor, Europhys.Lett. **9**, 701(1989).

[10] S. Sawada, Vacuum **41**, 612(1990); M. Kohyama, J.Phys. Condens.Matter **3**, 2193(1991); J.L. Mercer and M.Y. Chou, Phys.Rev.B **47**, 9366(1993); I. Kwon *et al*, Phys.Rev.B **49**, 7242(1994).

[11] We calculate the *ab initio* band structure of Silicon using the state-of-the-art self-consistent approach based on DFT,LDA, with norm conserving pseudopotentials and a plane wave basis set corresponding to a kinetic energy cut off of 24 Ry. We used 6 Chadi-Cohen points for Brillouin zone integration.

[12] See S.G.Louie, Phys.Rev.B **22**, 1933(1980) for the sp^3s^* basis set; inclusion of next-nearest-neighbours as a way to improve conduction bands was first proposed by D.J.Chadi and M.L.Cohen, Phys.Status Solidi B **68**, 405(1975).

[13] J. Donohue, *The Structure of the Elements*, (John Wiley & Sons, 1974).

[14] A.T. Paxton and A.P. Sutton, Acta. Metall. **37**, 1693(1989).

[15] M.T. Yin and M.L. Cohen, Phys.Rev.B **26**, 5668(1982); Phys.Rev.Lett. **45**, 1004(1980).

[16] H.J. Monkhorst and J.D. Pack, Phys.Rev.B **13**, 5188(1976).

[17] C.L. Fu and K.M. Ho, Phys.Rev.B **28**, 5480(1983).

[18] F.D. Murnagham, Proc.Nat.Acad.Sci.U.S.A. **30**, 244(1944).

[19] E. Roger Cowley, Phys.Rev.Lett. **60**, 2379(1988).

[20] F.S. Khan and J.Q. Broughton, Phys.Rev.B **39**, 3688(1989); C.Z. Wang, C.T. Chan and K.M. Ho, Phys.Rev.B **39**, 8586(1989).

[21] P.E. Blöchl and M.Parrinello, Phys.Rev.B **45**, 9413(1992).

[22] S. Nosé, Mol. Phys. **57**, 187(1986) and references therein.

[23] H.C. Andersen, J.Chem.Phys. **72**, 2384(1980).

[24] M. Parrinello and A. Rahman, Phys.Rev.Lett. **45**, 1196(1980)

[25] P. Focher *et al.*, Europhys. Lett. **36**, 345(1994).

[26] W.C. Swope *et al.*, Jnal.Chem.Phys. **76**, 637(1982).

[27] D.J. Chadi, Phys.Rev.Lett. **43**, 43(1979); M.T. Yin and M.L. Cohen, Phys.Rev.B **24**, 2303(1981).

[28] W.S. Yang, F. Jona and P.M. Marcus, Phys.Rev. B, **28**, 2049(1983); R.M. Tromp, R.G. Smeenk and F.W. Saris, Phys.Rev.Lett. **46**, 939(1981); M. Aono *et al.*, Phys.Rev.Lett. **49**, 567(1982).

[29] R.M. Tromp, R.J. Hamers and J.E. Demuth, Phys.Rev.Lett. **55**, 1303(1995); R.A. Wolkow, Phys.Rev.Lett. **68**, 2636(1992).

[30] J. Dabrowski and M. Scheffler, Appl.Surf.Sci. **56-58**, 15(1992).

[31] J.A. Applebaum and D.R.Hamann, Surf.Sci. **74**, 21(1978).

[32] J.E. Northrup, Phys.Rev.B **47**, 10032(1993).

[33] D.J. Chadi, Jnal.Vac.Sci.Technol. **16**, 1290(1979).